Article
Chinese Science Bulletin
SPECIAL ISSUE
Bulk Metallic Glasses
December 2011 Vol.56 No.36: 3926–3931
doi: 10.1007/s11434-011-4763-x

# Effect of Sn addition on the glass-forming ability and mechanical properties of Ni-Nb-Zr bulk metallic glasses

LI DengKe[1,2], ZHANG HaiFeng[1*], WANG AiMin[1], ZHU ZhengWang[1] & HU ZhuangQi[1]

[1] *Shenyang National Laboratory for Materials Science, Institute of Metal Research, Chinese Academy of Sciences, Shenyang 110016, China;*
[2] *Graduate University of the Chinese Academy of Sciences, Beijing 100049, China*

Received June 13, 2011; accepted August 10, 2011

The effect of tin (Sn) addition on the glass forming ability (GFA) and mechanical properties of the Ni-Nb-Zr ternary alloy system has been studied. The addition of Sn improves the GFA; $Ni_{61}Nb_{35.5-x}Zr_{3.5}Sn_x$ (in at.%) alloys with $x$=1 can be cast into amorphous samples at least 3 mm in diameter using a copper mold injection-casting method. The critical size for glass formation decreases to 2 mm when $x$=5 because $Ni_2SnZr$ phase precipitates readily. The addition of Sn is also effective in enhancing the stability of the supercooled liquid; a maximum supercooled liquid region of 48 K was attained for the $Ni_{61}Nb_{30.5}Zr_{3.5}Sn_5$ alloy. Compression tests reveal that the $Ni_{61}Nb_{33.5}Zr_{3.5}Sn_2$ alloy possesses the best mechanical properties, with yield strength ~3180 MPa, fracture strength ~3390 MPa and plastic strain ~1.3%. The fracture surfaces examined by scanning electron microscopy indicate that the alloys have a transition from ductility to brittleness in fracture behavior. The combination of high GFA, high thermal stability, high strength and compressive plasticity makes these alloys potentially attractive for engineering applications.

**metallic glasses, glass transition, thermal stability, mechanical properties**

**Citation:** Li D K, Zhang H F, Wang A M, et al. Effect of Sn addition on the glass-forming ability and mechanical properties of Ni-Nb-Zr bulk metallic glasses. Chinese Sci Bull, 2011, 56: 3926–3931, doi: 10.1007/s11434-011-4763-x

Bulk metallic glasses (BMGs) have attracted much attention from scientists and engineers over the past few decades, since they possess such promising properties as high yield strength, hardness and elastic strain limit, along with relatively high fracture toughness, fatigue resistance and corrosion resistance [1–3]. In the case of Ni-based alloys, glassy rods up to several millimeters in diameter have been successfully fabricated from many alloy systems, such as Ni-Nb-Cr-Mo-P-B [4], Ni-Zr-Ti-(Si,Sn) [5], Ni-Cu-Ti-Zr-Al [6], Ni-Nb-Zr [7], Ni-Nb-Sn [8], etc. These Ni-based bulk metallic glassy alloys have been reported to exhibit high strength (ranging up to 3000 MPa), high thermal stability (glass transition temperature generally around 880 K) [9,10], and excellent corrosion resistance [11]. The combination of superior properties enables them to have promising applications as engineering materials, such as for pressure sensors and micro-geared motors [12]. However, the achievement of a higher GFA for Ni-based amorphous alloys is still a challenging subject. So far the maximum dimension of Ni-based metallic glassy samples without noble elements is only 5 mm, which is much lower than that for other alloy systems, such as Zr-, Mg-, Ti-, Cu-, or Fe-based BMGs. Furthermore, most of the Ni-based BMGs exhibit a narrow supercooled liquid region (less than 40 K), which is not sufficient for processing. Thus, the development of new Ni-based BMGs with higher GFA as well as wide supercooled liquid region is of great importance.

It was reported that BMG samples up to 3 mm were fabricated in the Ni-Nb-Sn [8] and Ni-Nb-Zr [13] alloy systems. The composition regions for glass formation in these simple ternary systems are located in the range of $Ni_{60}Nb_{40-x}Sn_x$ ($3<x<9$) and $Ni_{61.5}Nb_{38.5-x}Zr_x$ ($0<x<9$), respectively. The atomic radii of Sn (0.162 nm) and Zr (0.160 nm) are nearly equivalent. The mixing enthalpies between the constituent elements are negative: –30, –49, –4 and –43 kJ/mol for Ni-Nb, Ni-Zr, Ni-Sn and Zr-Sn pairs, respectively [14].

*Corresponding author (email: hfzhang@imr.ac.cn)

According to Inoue's empirical rules for glass formation, it is reasonable to predict that the Ni-Nb-Zr-Sn quaternary system will exhibit high GFA. Actually, it has been reported that Sn could not only increase the GFA but also enhance the compression plasticity of some Cu- [15] and Ti-based BMGs [16,17]. In this paper, the effects of Sn addition on the GFA and mechanical properties of Ni-Nb-Zr alloys were systemically investigated.

## 1 Experimental

Alloy ingots with nominal compositions of $Ni_{61}Nb_{35.5-x}Zr_{3.5}Sn_x$ ($x$=0, 1, 2, 3, 4, 5, 6, 7 at.%) were prepared by arc melting a mixture of ultrasonically cleansed Ni, Nb, Zr and Sn elements with a purity of above 99.9% on a water-cooled Cu hearth under a Ti-gettered, high-purity argon atmosphere. Chemical homogeneity was ensured by repeated melting at least four times. The ingots were then remelted under high vacuum in a quartz tube by an induction heating coil and were injected through a nozzle with a diameter of 0.5–1 mm into a Cu mold to produce cylindrical samples 2–4 mm in diameter and 60 mm long. The structure was characterized by X-ray diffraction (XRD, Philips PW1050, Cu Kα). The thermal properties associated with the glass transition, crystallization and melting behaviors were studied by differential scanning calorimetry (DSC, Netzsch DSC 404C) at a heating rate of 20 K/min. Mechanical properties were measured using samples 2 mm in diameter and 4 mm long on a materials testing system (INSTRON5582). An MTS strain gauge was used to perform compression tests under a constant strain rate of $2\times10^{-4}$ $s^{-1}$. The fracture surfaces and master alloy ingots were examined by scanning electron microscopy (SEM, Hitachi S3400N).

## 2 Results

Figure 1(a) shows the XRD patterns taken from the cross section of the as-cast $Ni_{61}Nb_{35.5-x}Zr_{3.5}Sn_x$ ($x$ = 0, 1, 3, 5, 7 at.%) alloy rods with diameters of 2 mm. When $x$ varies from 0 to 5, the as-cast 2 mm diameter samples display only a series of diffuse maxima around $2\theta$=42°, and no clear diffraction patterns corresponding to crystalline phases are seen, indicating these samples are almost amorphous. When $x$=7, the XRD pattern of the 2 mm diameter as-cast rod exhibits apparent crystalline Bragg peaks, which are as attributed to NiNb, $NiNb_3$ and $Ni_2SnZr$ phases. Figure 1(b) shows the XRD patterns of the as-cast $Ni_{61}Nb_{35.5-x}Zr_{3.5}Sn_x$ ($x$=0, 1, 2, 3, 5 at.%) alloy rods with diameters of 3 mm. Only the $x$=1 alloy exhibits the broad diffraction peak characteristic of amorphous phase, indicating that the $Ni_{61}Nb_{34.5}Zr_{3.5}Sn_1$ alloy possesses the highest GFA. With higher Sn contents (e.g. $x\geqslant2$), $Ni_2SnZr$ phase begins to precipitate in addition to NiNb and $Ni_3Nb$ phases, which greatly deteriorate the GFA of these alloys.

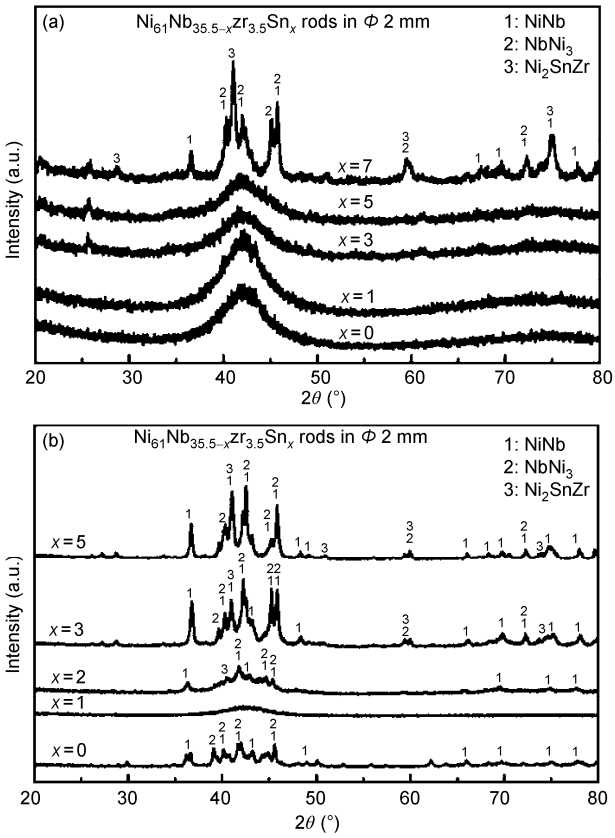


**Figure 1** XRD patterns of $Ni_{61}Nb_{35.5-x}Zr_{3.5}Sn_x$ alloy rods with diameters of (a) 2 mm and (b) 3 mm.

Figure 2 shows the high-temperature DSC profiles obtained from the as-cast glassy $Ni_{61}Nb_{35.5-x}Zr_{3.5}Sn_x$ ($x$=0, 1, 2, 3, 4, 5 at.%) alloy rods with diameters of 2 mm at a heating rate of 0.33 K/s under argon flow, showing the glass transition, crystallization and melting behaviors. All the alloys show clear glass transitions at the temperatures marked with arrows, followed by a super-cooled liquid region and crystallization, as shown in Figure 2(a). It is interesting to note that the two sub-peaks on the first crystallization peak when $x$=0, 1, 2 converge into one main peak when $x\geqslant3$, and a third tiny peak appears around 1200 K when $x\geqslant4$. The $T_g$ decreases slightly from 891 to 886 K while $T_x$ and $T_l$ increase gradually from 920 to 934 K and 1488 to 1505 K, respectively, with increasing Sn content. The temperature interval for the supercooled liquid region, $\Delta T_x = T_x - T_g$, also increases from 28 K when $x$=0 to 48 K when $x$=5. The thermal parameters are listed in Table 1, where $T_{rg}$ [18] is the reduced glass transition temperature, defined by the ratio of the $T_g$ to the melting temperature $T_l$, and $\gamma$ [19] is defined as $T_x/(T_g+T_l)$. Although γ is thought to have a strong correlation with the GFA, no correlation is seen here. However, $T_{rg}$ may be a better criterion for evaluating the GFA in the present alloy system.

Figure 3 shows the nominal compressive stress-strain curves of the as-cast 2 mm diameter BMG samples of the

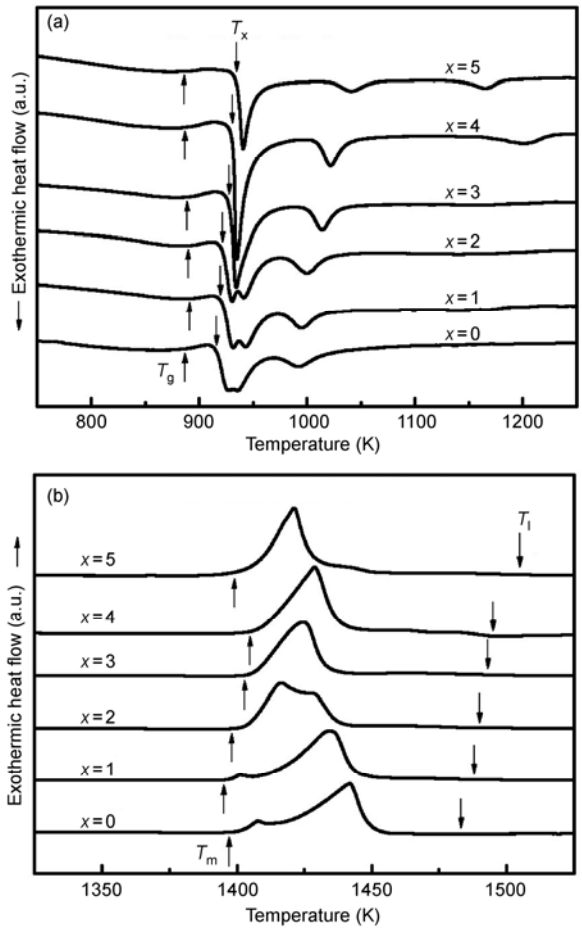


**Figure 2** DSC curves of $Ni_{61}Nb_{35.5-x}Zr_{3.5}Sn_x$ alloys, showing glass transition (a) and crystallization (b) melting events.

**Table 1** Critical diameter $D_c$ and thermal parameters for the Ni-Nb-Zr-Sn alloys

| Alloy | $D_c$ (mm) | $T_g$ (K) | $T_x$ (K) | $T_l$ | $\Delta T_x$ | $T_{rg}$ | $\gamma$ |
|---|---|---|---|---|---|---|---|
| $Ni_{61}Nb_{35.5}Zr_{3.5}$ | 2.5 | 887 | 915 | 1483 | 28 | 0.598 | 0.386 |
| $Ni_{61}Nb_{34.5}Zr_{3.5}Sn_1$ | 3 | 891 | 920 | 1488 | 29 | 0.599 | 0.387 |
| $Ni_{61}Nb_{33.5}Zr_{3.5}Sn_2$ | 2.5 | 890 | 922 | 1490 | 32 | 0.597 | 0.387 |
| $Ni_{61}Nb_{32.5}Zr_{3.5}Sn_3$ | 2.5 | 889 | 928 | 1493 | 39 | 0.595 | 0.390 |
| $Ni_{61}Nb_{31.5}Zr_{3.5}Sn_4$ | 2 | 887 | 931 | 1495 | 44 | 0.593 | 0.391 |
| $Ni_{61}Nb_{30.5}Zr_{3.5}Sn_5$ | 2 | 886 | 934 | 1505 | 48 | 0.589 | 0.391 |
| $Ni_{61}Nb_{34}Zr_4Sn_1$ | 3 | 887 | 920 | 1483 | 33 | 0.598 | 0.388 |

$Ni_{61}Nb_{35.5-x}Zr_{3.5}Sn_x$ ($x$=0, 1, 2, 3, 4 at.%) alloys. It is seen that for $x$=1 or 2, BMG samples display elastic deformation up to a strain of about 2.5% and an extremely high yield stress of about 3180 MPa, followed by some plastic deformation prior to ultimate fracture. The final stage of plastic deformation appears as a serrated fluctuation feature, which is also typical for BMGs. This phenomenon has been explained by the motion of localized shear bands formed under uniaxial compression [20]. At $x$=2, the fracture strength reaches a maximum value of about 3390 MPa, along with a plastic strain of about 1.3%. However, no obvious plasticity

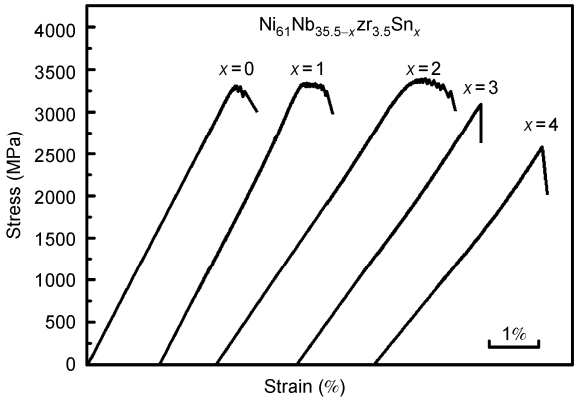


**Figure 3** Nominal compressive stress-strain curves for the $Ni_{61}Nb_{35.5-x}Zr_{3.5}Sn_x$ BMG alloys.

could be observed for alloys with $x$=3 and $x$=4, which is quite similar to the premature failure previously reported for Ni-Nb-Sn BMGs [21]. The fracture strengths for these five alloys shown are 3300, 3340, 3390, 3100 and 2580 MPa, respectively.

Figure 4 shows the fractographic morphologies of the $Ni_{61}Nb_{33.5}Zr_{3.5}Sn_2$ and $Ni_{61}Nb_{32.5}Zr_{3.5}Sn_3$ BMG samples. Figure 4(a) presents part of the fractured $Ni_{61}Nb_{33.5}Zr_{3.5}Sn_2$ specimen, exhibiting a shear plane induced by shear deformation. The vein-like patterns (Figure 4(b)), which are typical in fracture morphologies of glassy alloys, are observed. Significant development of vein patterns confirms plastic flow before failure. In addition, localized melting and protruded viscous flow (Figure 4(c)) along the fracture surface are observed, indicating a significant rise in temperature during final fracture [22,23]. However, the deformation behaviors observed for the $x$=3, 4 alloys are very different from those with $x$=1, 2. Flat facets and flutes with fatal cracks are observed on the fracture surface, as shown in Figure 4(d); these are generally features of brittle materials

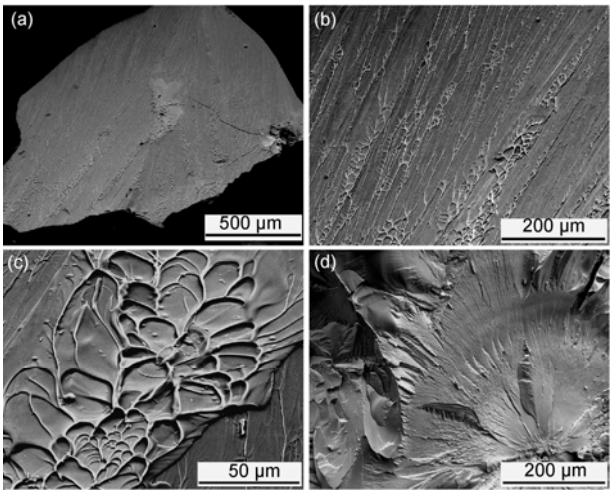


**Figure 4** SEM images of fracture surfaces. (a)–(c) $Ni_{61}Nb_{33.5}Zr_{3.5}Sn_2$; (d) $Ni_{61}Nb_{32.5}Zr_{3.5}Sn_3$.

such as Mg- and Fe-based BMGs [24]. It can be concluded that the alloys have a transition from ductility to brittleness when the Sn content increases from 2 to 3 at.%. Similar observations have also been reported in TiCuZrNiSn [16] and TiZrCuPdSn [17] alloy systems.

Figure 5 shows the backscattered SEM images of master alloy ingots of the $Ni_{61}Nb_{35.5-x}Zr_{3.5}Sn_x$ ($x$=0, 1, 2, 4, 7) alloy series. As indicated in Figure 5(a), the structure of the $Ni_{61}Nb_{35.5}Zr_{3.5}$ alloy is off-eutectic, with the long thin lathy bars as primary dendrites and the residual eutectic phases. From the phase diagram and the XRD analysis we determined that the lathy dendrites are $Ni_3Nb$ phase and the residual eutectic comprises $Ni_3Nb$ and NiNb phases. Figure 5(c) and (d) shows the microstructure of the $Ni_{61}Nb_{33.5}Zr_{3.5}Sn_2$ alloy at low and high magnification, respectively. A bright white phase of about 2 μm in size appears, distributed within the eutectic structures, as illustrated by the "C" in Figure 5(d). According to EDS and XRD analyses, the bright white phase is $Ni_2SnZr$. With increasing Sn additions, the $Ni_2SnZr$ phase begins to precipitate in large amounts, as shown in Figure 5(e) and (f). The chemical compositions of the phases shown in Figure 5(d) and (e) as well as their normalized composition are given in Table 2.

## 3 Discussion

As shown in Table 1, the supercooled liquid region is greatly increased with Sn addition, because of the slight decrease of $T_g$ and increase of $T_x$. The GFA reaches a maximum at 1 at.% Sn addition, while further Sn additions

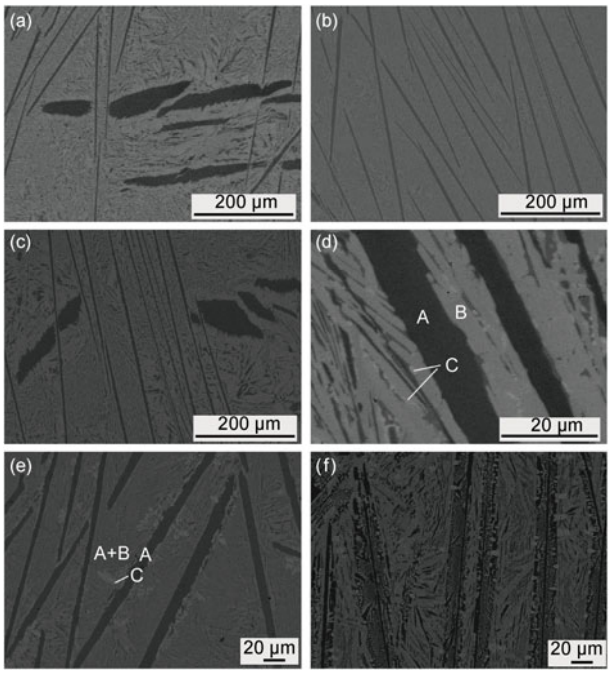


**Figure 5** Backscattered SEM images of the $Ni_{61}Nb_{35.5-x}Zr_{3.5}Sn_x$ master alloy ingots. (a) $x$=0; (b) $x$=1; (c), (d) $x$=2; (e) $x$=4; (f) $x$=7.

**Table 2** Chemical compositions of the phases in $Ni_{61}Nb_{33.5}Zr_{3.5}Sn_2$ and $Ni_{61}Nb_{31.5}Zr_{3.5}Sn_4$ alloys

| Alloy | Phase | Composition (at.%) | | | | Normalized phase |
|---|---|---|---|---|---|---|
| | | Ni | Nb | Zr | Sn | |
| $Ni_{61}Nb_{33.5}Zr_{3.5}Sn_2$ | A | 76.15 | 22.70 | 0.99 | 0.16 | $Ni_3Nb$ |
| | B | 53.62 | 43.90 | 0.22 | 2.26 | NiNb |
| | C | 49.70 | 4.22 | 22.57 | 23.51 | $Ni_2SnZr$ |
| $Ni_{61}Nb_{31.5}Zr_{3.5}Sn_4$ | A | 73.59 | 26.05 | 0.19 | 0.17 | $Ni_3Nb$ |
| | B | 50.29 | 45.10 | 0.19 | 4.42 | NiNb |
| | C | 47.93 | 5.98 | 21.17 | 24.92 | $Ni_2SnZr$ |

reduce the GFA. The large atomic size differences between Ni (0.123 nm) and Nb, Zr or Sn (0.143, 0.160 and 0.162 nm, respectively) can produce an efficiently packed local structure, which is often associated with low energy and high viscosity of liquids [25]. Moreover, the mixing enthalpies of Ni-Nb, Ni-Zr, Ni-Sn, Nb-Sn, Nb-Zr and Zr-Sn pairs are −30, −49, −4, −1, 4 and −43 kJ/mol, respectively. This shows that the bonding between Ni-Zr, Zr-Sn and Ni-Nb pairs is stronger than that between Ni-Sn, Nb-Zr and Nb-Sn, implying that Ni and Zr as well as the large atoms Zr and Sn have a tendency to cluster, which would make inter-atomic diffusion difficult. This would enhance the stability of the supercooled liquid, inducing the increase in $T_x$ and $\Delta T_x$. After a careful comparison between Figure 5(a) and (b), it can be deduced that the primary $Ni_3Nb$ phase is refined and the formation of residual eutectic phase is greatly hindered by the substitution of 1 at.% Sn for Nb in $Ni_{61}Nb_{35.5}Zr_{3.5}$ alloy. The nucleation of $Ni_3Nb$ phase is restricted, since the compositional fluctuations required are more difficult to realize after addition of Sn element, which has a very limited solubility in the $Ni_3Nb$ phase, as indicated by the 0.16 and 0.17 at.% Sn contents of $Ni_3Nb$ phase in the $Ni_{61}Nb_{33.5}Zr_{3.5}Sn_2$ and $Ni_{61}Nb_{31.5}Zr_{3.5}Sn_4$ alloys (Table 2), respectively. The growth of primary $Ni_3Nb$ phase requires diffusion of Sn element from the solid-liquid interface, which would reduce the growth rate and result in enrichment of Sn element in the undercooled melt. The subsequent eutectic solidification process would also be hampered since the cooperative growth of eutectic structure requires diffusion and redistribution of Sn element between different phases. For excessive Sn addition ($x$>1), the solidification of $Ni_3Nb$ phase would result in great enrichment of Sn element in some local areas, causing easy precipitation of $Ni_2SnZr$ phase at these sites, as illustrated in Figure 5(d). Furthermore, the rapid increase of liquidus temperatures with Sn addition may also play a dominant role in the deterioration of the GFA [26]. Therefore, the $Ni_{61}Nb_{34.5}Zr_{3.5}Sn_1$ alloy possesses the best GFA.

As also found in other studies [16,17], we have noticed that proper Sn addition could significantly improve the compression plasticity of the alloys. It has been widely accepted that the plasticity of BMGs depends on the generation of multiple shear bands. Structural inhomogeneities,

such as nanocrystals, medium-range ordering, and phase separation, can be considered to induce the initiation and propagation of shear bands [27,28]. As pointed out in reference [29], a large difference in enthalpy of mixing between atom pairs in the multi-component Ni-Nb-Zr-Sn alloys may promote structures that differ greatly from a homogeneous atomic arrangement, causing atomic-scale structural inhomogeneity and/or locally favored structures. The atomic-scale chemical ordering can improve the local packing density and hinder long-range diffusion of atoms [30]. As a consequence, appropriate addition of Sn could simultaneously improve the glass forming ability and compressive plasticity. However, when more than 2 at.% Sn is added, the compressive deformation behavior changes abruptly [31], transforming from ductility to brittleness, as exemplified in Figure 3. Zhang et al. [32] have observed that the plasticity of BMGs in the Zr-Cu-Al and Hf-Ni-Al alloy systems depends on composition, and ascribed the ductile-to-brittle transition to the composition-dependent internal structures that influence shear transformation and shear localization behavior under loading. Actually, the atomic-level structure of Ni-Nb-Zr alloys is changed significantly with addition of Sn, as can be deduced from the distinct evolution of the DSC profiles [33] in Figure 2. Therefore, we presume that excessive Sn addition may facilitate the formation of structural inhomogeneities or atomic-level ordering, and hinder the generation of shear transformation events [34]. Thus, the plastic strain is confined to a few shear bands, causing catastrophic brittle failure.

## 4 Conclusions

(1) Addition of Sn element is effective in enhancing the supercooled liquid region and increasing the GFA of Ni-Nb-Zr alloys. The maximum $\Delta T_x$ value is 48 K for $Ni_{61}Nb_{30.5}Zr_{3.5}Sn_5$ alloy and metallic glassy rods with diameter at least 3 mm could be obtained for the $Ni_{61}Nb_{34.5}Zr_{3.5}Sn_1$ alloy.

(2) The alloy $Ni_{61}Nb_{33.5}Zr_{3.5}Sn_2$ possesses the best mechanical properties with yield strength 3180 MPa, fracture strength 3390 MPa and plastic strain of 1.3%. The addition of Sn changes the local atomic environment of Ni-Nb-Zr alloys, developing structural inhomogeneities and/or atomic-level ordering, which may account for the significant compressive plasticity.

*This work was supported by the National Natural Science Foundation of China (50825402 and 50731005) and the National Basic Research Program of China (2011CB606301).*

1 Wang W H, Dong C, Shek C H. Bulk metallic glasses. Mater Sci Eng R, 2004, 44: 45–89
2 Zhang Q S, Wu S D, Zhang H F, et al. Cyclic fatigue fracture of $Zr_{55}Al_{10}Ni_5Cu_{30}$ bulk amorphous alloy with quenched-in crystallites. J Mater Sci Technol, 2003, 19: 13–15
3 Inoue A, Shen B L, Chang C T. Super-high strength of over 4000 MPa for Fe-based bulk glassy alloys in $[(Fe_{1-x}Co_x)_{0.75}B_{0.2}Si_{0.05}]_{96}Nb_4$ system. Acta Mater, 2004, 52: 4093–4099
4 Wang X M, Yoshii I, Inoue A, et al. Bulk amorphous $Ni_{75-x}Nb_5M_xP_{20-y}B_y$ (M=Cr, Mo) alloys with large supercooling and high strength. Mater Trans JIM, 1999, 40: 1130–1136
5 Yi S, Park T G, Kim D H. Ni-based bulk amorphous alloys in the Ni-Ti-Zr-(Si,Sn) system. J Mater Res, 2000, 15: 2425–2429
6 Xu D, Duan G, Johnson W L, et al. Formation and properties of new Ni-based amorphous alloys with critical casting thickness up to 5 mm. Acta Mater, 2004, 52: 3493–3497
7 Chen L Y, Hu H T, Zhang G Q, et al. Catching the Ni-based ternary metallic glasses with critical diameter up to 3 mm in Ni-Nb-Zr system. J Alloy Compd, 2007, 443: 109–113
8 Yim H C, Xu D H, Johnson W L. Ni-based bulk metallic glass formation in the Ni-Nb-Sn and Ni-Nb-Sn-*X* (*X*=B, Fe, Cu) alloy systems. Appl Phys Lett, 2003, 82: 1030–1032
9 Zhu Z W, Zhang H F, Pan D G, et al. Fabrication of binary Ni-Nb bulk metallic glass with high strength and compressive plasticity. Adv Eng Mater, 2006, 8: 953–957
10 Chen L Y, Fu Z D, Zeng W, et al. Ultrahigh strength binary Ni-Nb bulk glassy alloy composite with good ductility. J Alloy Compd, 2007, 443: 105–108
11 Zhu Z W, Zhang H F, Ding B Z, et al. Synthesis and properties of bulk metallic glasses in the ternary Ni-Nb-Zr alloy system. Mater Sci Eng A, 2008, 492: 221–229
12 Inoue A, Shen B L, Takeuchi A. Fabrication, properties and applications of bulk glassy alloys in late transition metal-based systems. Mater Sci Eng A, 2006, 441: 18–25
13 Zhu Z W, Zhang H F, Sun W S, et al. Effect of Zr addition on the glass-forming ability and mechanical properties of Ni-Nb alloy. J Mater Res, 2007, 22: 453–459
14 Takeuchi A, Inoue A. Calculations of mixing enthalpy and mismatch entropy for ternary amorphous alloys. Mater Trans JIM, 2000, 41: 1372–1378
15 Zhang Q S, Zhang H F, Deng Y F, et al. Bulk metallic glass formation of Cu-Zr-Ti-Sn alloy. Scripta Mater, 2003, 49: 273–278
16 Xie K F, Yao K F, Huang T Y. Preparation of $(Ti_{0.45}Cu_{0.378}Zr_{0.10}Ni_{0.072})_{100-x}Sn_x$ bulk metallic glass. J Alloy Compd, 2010, 504s: s22–s26
17 Zhu S L, Wang X M, Inoue A. Glass-forming ability and mechanical properties of Ti-based bulk glassy alloys with large diameters of up to 1 cm. Intermetallics, 2008, 16: 1031–1035
18 Turnbull D. Under what condition can a glass be formed? Contemp Phys, 1969, 10: 473–488
19 Lu Z P, Liu C T. A new glass-forming ability criterion for bulk metallic glasses. Acta Mater, 2002, 50: 3501–3512
20 Suo Z Y, Qiu K Q, Li Q F, et al. Effect of Nb on glass forming ability and plasticity of (Ti-Cu)-based bulk metallic glasses. Mater Sci Eng A, 2010, 527: 2486–2491
21 Yim H C, Xu D H, Lind M L, et al. Structure and mechanical properties of bulk glass-forming Ni-Nb-Sn alloys. Scripta Mater, 2006, 54: 187–190
22 Liu L F, Dai L H, Bai Y L, et al. Initiation and propagation of shear bands in Zr-based bulk metallic glass under quasi-static and dynamic shear loadings. J Non-Cryst Solids, 2005, 351: 3259–3270
23 Liu L F, Dai L H, Bai Y L, et al. Behavior of multiple shear bands in Zr-based bulk metallic glass. Mater Chem Phys, 2005, 93: 174–177
24 Xi X K, Zhao D Q, Pan M X, et al. Fracture of brittle metallic glasses: Brittleness or plasticity. Phys Rev Lett, 2005, 94: 125510
25 Xu D, Duan G, Johnson W L. Unusual glass-forming ability of bulk amorphous alloys based on ordinary metal copper. Phys Rev Lett, 2004, 92: 245504
26 Sun W S, Zhang H F, Ding B Z, et al. Relationship of glass formation ability and eutectics in ternary Ni-Zr-B system. J Mater Res, 2004, 19: 2523–2526
27 Hays C C, Kim C P, Johnson W L. Microstructure controlled shear band pattern formation and enhanced plasticity of bulk metallic

glasses containing in situ formed ductile phase dendrite dispersions. Phys Rev Lett, 2000, 84: 2901–2904
28 Das J, Tang M B, Kim K B, et al. "Work-hardenable" ductile bulk metallic glass. Phys Rev Lett, 2005, 94: 205501
29 Park E S, Chang H J, Kim D H. Effect of addition of Be on glass-forming ability, plasticity and structural change in Cu-Zr bulk metallic glasses. Acta Mater, 2008, 56: 3120–3131
30 Park E S, Chang H J, Lee J Y, et al. Improvement of plasticity by tailoring combination of constituent elements in Ti-rich Ti-Zr-Be-Cu-Ni bulk metallic glasses. J Mater Res, 2007, 22: 3440–3449
31 Fu H M, Zhang H F, Wang H, et al. Multifarious fracture features of CuZrAlGd (Ag) bulk metallic glasses. Adv Mat Res, 2007, 47: 29–30
32 Zhang L, Cheng Y Q, Cao A J, et al. Bulk metallic glasses with large plasticity: Composition design from the structural perspective. Acta Mater, 2009, 57: 1154–1164
33 Qin F X, Zhang H F, Wang A M, et al. Effect of Pd on GFA and thermal stability of Zr-based bulk amorphous alloy. J Mater Sci Technol, 2004, 20: 160–163
34 Cheng Y Q, Cao A J, Sheng H W, et al. Local order influences initiation of plastic flow in metallic glass: Effects of alloy composition and sample cooling history. Acta Mater, 2008, 56: 5263–5275